ELSEVIER

Journal of Organometallic Chemistry 579 (1999) 285–297

Journal of Organometallic Chemistry

Electron-deficient triruthenium and triosmium clusters from the reaction of the cluster anions $[HM_3(CO)_{11}]^-$ (M = Ru, Os) with tricyclohexylphosphine in methanol

Georg Süss-Fink [a,*], Isabelle Godefroy [a], Vincent Ferrand [a], Antonia Neels [a], Helen Stoeckli-Evans [a], Samia Kahlal [b], Jean-Yves Saillard [b], Maria Teresa Garland [c]

[a] *Institut de Chimie, Université de Neuchâtel, avenue de Bellevaux 51, CH-2000 Neuchâtel, Switzerland*
[b] *Laboratoire de Chimie du Solide et Inorganique Moléculaire, UMR-6511, Université de Rennes 1, F-35042 Rennes Cedex, France*
[c] *Laboratorio de Cristalografia, Universidad de Chile, Casilla 487-3, Santiago, Chile*

Received 10 December 1998

Abstract

The reaction of $Na[HRu_3(CO)_{11}]$ with an excess of tricyclohexylphosphine in methanol gives the neutral complex $H_2Ru_3(CO)_6(PCy_3)_3$ which is the first 44 e^- triruthenium cluster reported. This highly electron-deficient species reacts with carbon monoxide to give the saturated 48 e^- cluster $Ru_3(CO)_9(PCy_3)_3$. The electronic structure of the novel 44 e^- cluster was established by EHT and DFT molecular orbital calculations of isoelectronic model compounds. The analogous reaction of $[N(PPh_3)_2][HOs_3(CO)_{11}]$ with PCy_3 in methanol affords the 46 e^- cluster $H_2Os_3(CO)_7(PCy_3)_3$, the first trisubstituted derivative of $H_2Os_3(CO)_{10}$. In all cases methanol acts as source of protons for the formation of the hydrido clusters.

Keywords: Cluster; Trinuclear; Unsaturated; Phosphine; Hydrido

1. Introduction

Ligand substitution reactions of dodecacarbonyltriruthenium with tertiary phosphines have been studied in great detail [1]: the thermal reaction of $Ru_3(CO)_{12}$ with PR_3 in general leads to the mono-, di-, and trisubstituted derivatives $Ru_3(CO)_{11}(PR_3)$, $Ru_3(CO)_{10}(PR_3)_2$, $Ru_3(CO)_9(PR_3)_3$ [2]. For the directed synthesis of these substitution products, the radical ion-initiated ligand substitution [3,4], the bis(triphenylphosphine)iminium salt-catalysed carbonyl substitution [5,6], and the trimethylamine oxide-induced carbonyl substitution [7,8] have been developed. However, with sterically demanding phosphine ligands, the synthesis of the trisubstituted derivatives failed: even a 6-fold excess of tricyclohexylphosphine with $Ru_3(CO)_{12}$ in the presence of $[Na][Ph_2CO]$ gave only the mono- and the disubstituted complexes, but no $Ru_3(CO)_9(PCy_3)_3$ [4].

On the other hand, bulky phosphines containing cyclohexyl or *tert*-butyl substituents are known to allow unusual structures and unsaturated configurations for steric reasons [9,10]: thus the electron-deficient triruthenium cluster $H_2Ru_3(CO)_5(P^tBu_2)_2(Ph_2PCH_2PPh_2)$ with an electron count of 46 e^- was synthesised by Böttcher et al. in 1996 [10]. Apart from this complex and its adamantyl derivative [10], the only electron-deficient Ru_3 clusters reported prior to this work are $HRu_3(CO)_9(PPh_2)$ [11], $Ru_3(CO)_7(PhCCPh)(Ph_2PCH_2PPh_2)$ [12], $HRu_3(CO)_7(C_{12}H_{10})$ [13], $HRu_3(CO)_9(NSOMePh)$ [14], and $H_2Ru_3(CO)_{10}$ as well as its phosphine derivative $H_2Ru_3(CO)_9(PPh_3)$ [15], all of them with an

* Corresponding author. Tel.: +41-32-7182400; fax: +41-32-7182511.
E-mail address: suess-fink@ich.unine.ch (G. Süss-Fink)

0022-328X/99/$ - see front matter
PII: S0022-328X(99)00011-X

electron count of 46 e^-. Interestingly, no unsaturated triruthenium cluster is mentioned in Deeming's review of 1995 [1].

In a preliminary communication [16] we reported the serendipitic isolation and characterisation of the clusters $H_2Ru_3(CO)_6(PCy_3)_3$ and $Ru_3(CO)_9(PCy_3)_3$ from the reaction of $[HRu_3(CO)_{11}]^-$ with tricyclohexylphosphine. We know describe the rational synthesis, the interrelations, and the detailed X-ray structure characterisation of those clusters as well as the analogous reaction of $[HOs_3(CO)_{11}]^-$ leading to $H_2Os_3(CO)_7(PCy_3)_3$.

2. Synthetic and crystallographic results

The thermal reaction of the cluster anion $[HRu_3(CO)_{11}]^-$ (**1**) with an excess of tricyclohexylphosphine in methanol leads, depending on the reaction conditions, to two different neutral clusters: in an open reaction vessel, the hydrido cluster $H_2Ru_3(CO)_6(PCy_3)_3$ (**3**) is obtained, while in a closed reactor the cluster $Ru_3(CO)_9(PCy_3)_3$ (**5**) is formed. Both compounds precipitate directly from the reaction mixture and can be isolated by filtration in high yields.

The neutral clusters **3** and **5** form from the cluster anion $[HRu_3(CO)_{11}]^-$ (**1**) in thoroughly dried methanol (ultra pure grade) under rigorous exclusion of air and moisture. Addition of water to the reaction mixture causes a decrease in the yields of **3** and **5**. We therefore conclude that the methanol not only is the solvent but also acts as a source of protons in the reaction with **1**. The strong influence of the reaction condition (closed or open reactor) on the product formation is due to the presence or absence of carbon monoxide resulting from the substitution of carbonyl ligands by the phosphine. Thus, we were able to show that **3** converts into **5** under CO pressure.

On the basis of these findings, we propose the reaction sequence summarised in Scheme 1: in the first step, three carbonyl ligands in **1** are replaced by three phosphine ligands to give the intermediate anion $[HRu_3(CO)_8(PCy_3)_3]^-$ (**2**) which, however, could not be detected in the reaction mixture. It seems to react immediately with methanol to give, in a open reactor, the unsaturated dihydro cluster $H_2Ru_3(CO)_6(PCy_3)_3$ (**3**). In a closed reactor, the carbon monoxide pressure inhibits the further elimination of CO and affords, with elimination of H_2, the saturated cluster $Ru_3(CO)_9(PCy_3)_3$ (**5**). The isolated unsaturated cluster **3** reacts in dichloromethane with carbon monoxide (1.5 bar) to give an intermediate which could be characterised by NMR spectroscopy to be most likely a saturated dihydro complex $H_2Ru_3(CO)_9(PCy_3)_3$ (**4**). The red intermediate **4** converts, slowly in CH_2Cl_2 solution but spontaneously on silica gel or alox, into the violet

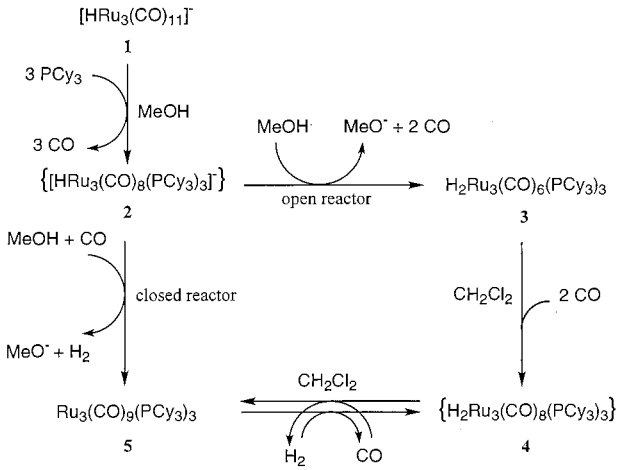

Scheme 1. Reaction of $[HRu_3(CO)_{11}]^-$ (**1**) with PCy_3 in methanol. The intermediate {4} is characterised in solution, species {2} is hypothetical.

compound **5**. On the other hand, **5** reacts with molecular hydrogen (1.5 bar) in CH_2Cl_2 solution at room temperature to give **4**.

The trinuclear clusters **3** and **5**, which precipitate in a pure form directly from the corresponding reaction solution, are recrystallised from a mixture of dichloromethane and methanol to give, in all cases, red crystals suitable for X-ray diffraction. Their spectroscopic (IR, MS, ^{1}H-and ^{31}P-NMR) and analytical data, given in Section 4, are in accordance with the structure found by X-ray crystallography (Fig. 1).

The single-crystal X-ray structure analysis of $H_2Ru_3(CO)_6(PCy_3)_3$ (**3**) shows a Ru_3 skeleton bearing two μ_3-hydrido caps, on either side of the triangle. The three Ru–Ru bonds are bridged by three μ_2-carbonyl ligands being almost in the plane of the metal triangle. The three terminal carbonyls as well as the three phosphine ligands are coordinated to the three ruthenium atoms, above and below the metal plane. Important bond lengths and angles are given in Table 1.

The three Ru–P bonds [2.332(2), 2.336(2), 2.344(2) Å] are very similar in length. The three Ru–C bonds of the three terminal carbonyl ligands (1.834(7), 1.834(7), 1.825(8) Å) are shorter than those in $Ru_3(CO)_{12}$ (eq: 1.921(5), ax: 1.942(4) Å) [17]. The bridging carbonyls

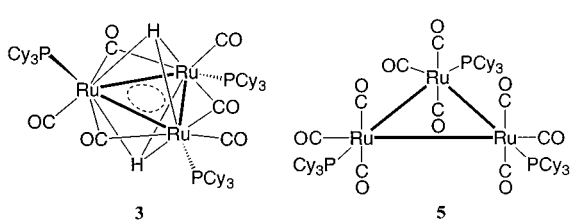

Fig. 1. Structural plots of the 44 e^- $H_2Ru_3((CO)_6(PCy_3)_3$ (**3**) and the 48 e^- cluster $Ru_3((CO)_9(PCy_3)_{3d}$ (**5**).

Table 1
Selected bond lengths (Å) and angles (°) for $H_2Ru_3(CO)_6(PCy_3)_3$ (**3**)

Bond lengths[a]		Angles[a]	
Ru(1)–Ru(2)	2.6702(6)	Ru(2)–Ru(1)–Ru(3)	59.97(2)
Ru(1)–Ru(3)	2.7180(7)	Ru(1)–Ru(2)–Ru(3)	60.90(2)
Ru(2)–Ru(3)	2.6931(7)	Ru(2)–Ru(3)–Ru(1)	59.14(2)
Ru(1)–P(1)	2.332(2)	H(1)–Ru(1)–P(1)	101.0
Ru(2)–P(3)	2.336(2)	H(1)–Ru(2)–P(3)	168.3
Ru(3)–P(2)	2.344(2)	H(1)–Ru(3)–P(2)	104.4
Ru(1)–H(1)	1.94	H(2)–Ru(1)–P(1)	172.6
Ru(1)–H(2)	1.61	H(2)–Ru(2)–P(3)	104.7
Ru(2)–H(1)	2.04	H(2)–Ru(3)–P(2)	171.8
Ru(2)–H(2)	1.94	C(4)–Ru(1)–P(1)	91.1(2)
Ru(3)–H(1)	1.93	C(6)–Ru(2)–P(3)	92.3(2)
Ru(3)–H(2)	1.85	C(5)–Ru(3)–P(2)	88.2(2)
Ru(1)–C(4)	1.834(7)		
Ru(2)–C(6)	1.834(7)		
Ru(3)–C(5)	1.825(8)		
Ru(1)–C(1)	2.134(7)		
Ru(3)–C(1)	2.161(6)		
Ru(2)–C(2)	2.107(7)		
Ru(3)–C(2)	2.147(5)		
Ru(1)–C(3)	2.154(6)		
Ru(2)–C(3)	2.129(6)		

[a] Estimated standard deviations in parantheses.

are coordinated unsymmetrically, the Ru–C distances (2.134(7), 2.161(6), 2.107(7), 2.147(5), 2.154(6), 2.129(6) Å) being in the usual range of ruthenium carbonyl bridges (2.073–2.219 Å) [18] (Fig. 2).

The two capping hydrido ligands are unsymmetrically coordinated, H(2) being closer to the Ru_3 triangle than H(1). The different environment (one PCy_3 and two CO ligands surrounding H(2), two PCy_3 and one CO ligands surrounding H(1)) is also reflected in ^{1}H-NMR spectrum of **3**, where two different hydride resonances are observed, both showing a homo-spin coupling to the other one and two hetero-spin couplings to the three phosphorus atoms. The signal at δ −19.46 ppm (doublet of triplets of doublets), assigned to H(1), shows a large coupling (28.3 Hz) to P(3) and a smaller coupling (5.3 Hz) to P(1) and P(2), apart from H(1)–H(2) coupling of 2.2 Hz. The larger coupling to P(3) is presumably due to the large H(1)–Ru(2)–P(3) angle (168.3°) with respect to the smaller angles H(1)–Ru(1)–P(1) and H(1)–Ru(3)–P(2) which measure 101.0 and 104.4°, respectively. The second signal, attributed to H(2), appears as a triplet of doublets of doublets at δ −21.02 ppm. It shows a large coupling (26.4 Hz) to the two phosphorus atoms P(1) and P(2), the angle H(2)–Ru(1)–P(1) and H(2)–Ru(3)–P(2) being 172.6 and 171.8°, respectively. The smaller hetero-spin coupling (5.4 Hz) is with P(3) because of the smaller H(2)–Ru(2)–P(3) angle 104.7°.

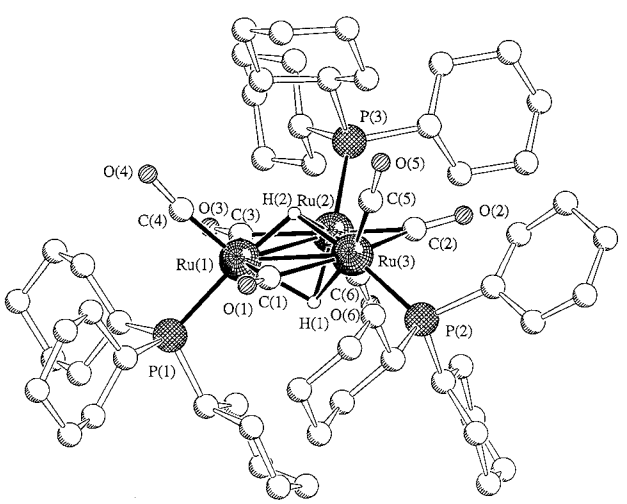

Fig. 2. Molecular structure of $H_2Ru_3((CO)_6(PCy_3)_3$ (**3**). The hydrogen atoms of the cyclohexyl groups have been omitted for clarity.

Complex **3** is, to our knowledge, the only Ru_3 cluster known presenting an electron count of 44 e^-. Trinuclear clusters with 44 e^- have been reporting so far only for d^{10} and d^6 metals: $[Pd_3(SO_2)_2(t\text{-BuNC})_5]$ [19], $[Pt_3(CO)_3(P(C_6H_{11})_3)_4]$ [20], $Pd_3(P^tBu_2)_3(CO)_2Cl$ [21], $Pt_3(PPh_2)_3(PPh_3)_2Ph$ [22], $Pt_3(SO_2)_3(dppp)(PCy_3)_2$ [23], $[Pt_3(SO_2)_2(PCy_3)_3Br]^-$ [24], $[Pd_3(PPh_2)_2(PEt_3)_3Cl]^+$ [25], $[Pd_3(PPh_2)_2(PPh_3)_3Cl]^+$ and $[Pd_2Pt(PPh_2)_2(PPh_3)_3Cl]^+$ [26], $[H_3Pt_3(dppm)_3\{P(OMe)_3\}_3]^+$ [27], $[FePt_2(CO)_5^-(P(OPh)_3)_3]$ [28], $Cr_3(dppe)_3S_5$ [29], $Mo_3(PMe_3)_6S_5$ [30], $[Mo_3Cl_9S_5]^{3-}$ [31], $[W_3(OOCCH_3)_6(H_2O)_3O]^{2+}$ [32]. In accordance with the high electron-deficiency, the Ru–Ru bonds in **3** are found to be rather short (2.6702(6), 2.6931(7) and 2.7180(7) Å) with respect to the typical Ru–Ru single bonds of (2.9396(8) Å) in **5** (see below). In addition, the Ru–P bonds in **3** (2.332(2), 2.336(2) and 2.344(2)Å) are also shorter then in **5** (2.414(2) Å). The electron deficiency of **3** (four electrons missing with respect to the noble gas rule) is expressed by a dotted circle within the Ru_3 triangle (Figs. 1 and 3).

The single-crystal X-ray structure analysis of $Ru_3(CO)_9(PCy_3)_3$ (**5**) reveals a triruthenium framework with the three phosphine ligands occupying equatorial positions at the three ruthenium atoms. The nine carbonyl ligands are all terminal, six occupying the two axial positions of the Ru atoms, while the other three are alternating with the phosphine ligands in one of the two equatorial positions of each ruthenium atom. The $Ru–CO_{eq}$ distances being 1.876(7) Å are distinctly shorter than the $Ru–CO_{ax}$ distances (1.924(7) and 1.931(7) Å). This is in line with the findings in the known cluster $Ru_3(CO)_9(PMe_3)_3$ [16], the Ru–P distances, however, are considerably longer in **5** (2.414(2) Å) than in the methyl derivative (2.330 Å (average)) [33], reflecting the bulkiness of the cyclohexyl substituents. The Ru–Ru bonds in **5** (2.9396(8) Å) are also elongated with respect to those in $Ru_3(CO)_9(PMe_3)_3$ (2.860(1), 2.862(1), 2.854(1) Å) [33] and in $Ru_3(CO)_{12}$

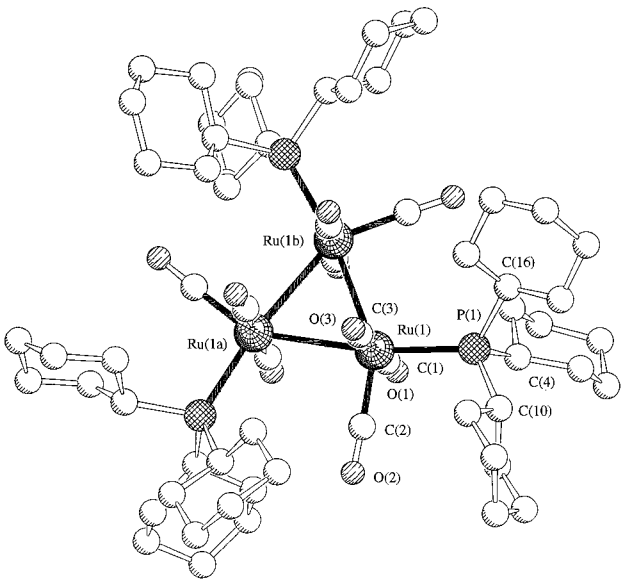

Fig. 3. Molecular structure of $Ru_3((CO)_9(PCy_3)_3$ (**5**). The hydrogen atoms of the cyclohexyl groups have been omitted for clarity.

(2.852(1), 2.851(1), 2.860(1) Å) [17]. The molecule **5** has almost D_{3h} symmetry, the three phosphorus atoms being almost in the plane of the three ruthenium atoms (maximum distance between P and the Ru_3 plane 0.20 Å) and the torsion angles C(axial)–Ru–Ru–C(axial) being less than 10° (Table 2).

The intermediary cluster **4** is observed in the reaction of the 44 e$^-$ cluster $H_2Ru_3(CO)_6(PCy_3)_3$ (**3**) with carbon monoxide (1.5 bar) in dichloromethane to give the 48 e$^-$ cluster $Ru_3(CO)_9(PCy_3)_3$ (**5**). It is also obtained from the reaction of **5** with molecular hydrogen (1.5 bar) in dichloromethane. Because of its rapid decomposition to **5**, it was not possible to isolate **4**; it could only be characterised by mass spectroscopy and its IR and NMR data in solution. On the basis of these data (see Section 4) and the noble gas rule (electron count 48 e$^-$), and in the light of **4** being an intermediate in the reaction of **3** to **5**, we propose **4** to have the composition $H_2Ru_3(CO)_8(PCy_3)_3$ (Fig. 4). The IR spectrum of **4** shows three absorptions in the region of the terminal carbonyl ligands only. In the ^{1}H-NMR spectrum, apart from the multiplet of the cyclohexyl substituents, **4** gives rise to two hydride resonances: the signal at δ

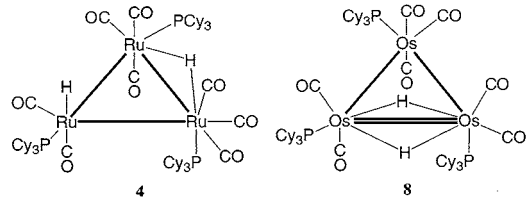

4 8

Fig. 4. Proposed structure of the 48 e$^-$ cluster $H_2Ru_3((CO)_8(PCy_3)_3$ (**4**) and structural plot of the 46 e$^-$ cluster $H_2Os_3((CO)_7(PCy_3)_3$ (**8**).

-17.94 ppm, a doublet of doublets is coupled to two different phosphorus atoms (20.2 and 7.6 Hz) one being equatorial and the other on being axial, but not to the third one nor to the other hydride; it is assigned to the bridging hydrido ligand. The second signal at δ -10.89 ppm is assigned to a terminal hydride; it appears as a doublet and shows only a coupling to one phosphorus atom (10 Hz). The 48 e$^-$ cluster $H_2Ru_3(CO)_8(PCy_3)_3$ which we propose for the intermediate **4** observed in solution is a derivative of the parent compound $H_2Ru_3(CO)_{11}$ obtained by Keister et al. from the protonation of $[HRu_3(CO)_{11}]^-$ at low temperature; this cluster was also characterised spectroscopically in solution and could not be isolated [34,35]. Very recently, $H_2Ru_3(CO)_{11}$ has been prepared by reaction of $Ru_3(CO)_{11}$(NCMe) with H_2 and carefully characterised by ^{1}H- and ^{13}C-NMR spectroscopy [36]. For **4** additional evidence comes from the ^{31}P-NMR spectrum showing three resonances for the three different phosphine ligands, and from the mass spectrum (ESI positive) showing a molecular peak at 1372 (calculated for ^{102}Ru) with the correct Ru_3 isotope pattern.

The reaction of the osmium analogue $[HOs_3(CO)_{11}]^-$ (**6**) with an excess of tricyclohexylphosphine (1:5) in methanol leads, upon heating to 80°C for 3 h, to the neutral cluster $H_2Os_3(CO)_7(PCy_3)_3$ (**8**) which precipitates directly from the reaction solution. The possible anionic intermediate $[HOs_3(CO)_8(PCy_3)_3]^-$ (**7**) could not be detected in solution (Scheme 2). Also in this case, methanol acts as a source of protons, since the highest yield is obtained with thoroughly dried methanol and in the absence of air and moisture.

The complex $H_2Os_3(CO)_7(PCy_3)_3$ (**8**) has an electron count of 46 electrons and derives from the famous unsaturated osmium cluster $H_2Os_3(CO)_{10}$ [37,38] the

Table 2
Selected bond lengths (Å), angles (°) and torsion angles (°) for $Ru_3(CO)_9(PCy_3)_3$ (**5**)

Bond lengths[a]		Angles[a]		Torsion angles[a]	
Ru(1)–Ru(1a)	2.9396(9)	Ru(2)–Ru(1)–Ru(3)	60.0	C(1)–Ru(1)–Ru(1a)–C(1a)	0
Ru(1)–P(1)	2.414(2)	Ru(3)–Ru(1)–P(1)	111.22(5)	C(1)–Ru(1)–Ru(1a)–C(1a)	3.6(3)
Ru(1)–C(1)	1.923(7)	P(1)–Ru(1)–C(2)	98.2(2)		
Ru(1)–C(2)	1.876(7)	P(1)–Ru(1)–C(1)	92.0(2)		
Ru(1)–C(3)	1.931(7)	P(1)–Ru(1)–C(3)	90.2(4)		

[a] Estimated standard deviations in parentheses. Symmetry code: (a) *y*,*z*,*x*.

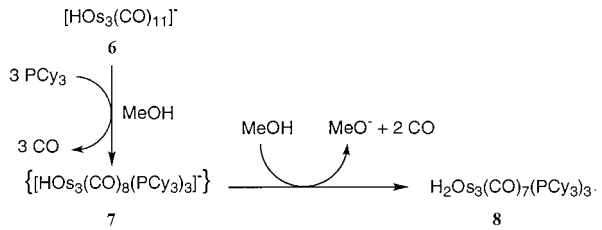

Scheme 2. Reaction of $[HOs_3(CO)_{11}]^-$ (**6**) with PCy_3 in methanol. The intermediate {**7**} is hypothetical.

chemistry of which has been studied in great detail [39]. To our knowledge, **8** is the only trisubstituted derivative of $H_2Os_3(CO)_{10}$ reported so far; Deeming's comprehensive review of 1995 mentions only monosubstituted derivatives [1].

Complex **8** is characterised by spectroscopic and analytical data (see Section 4) and by X-ray diffraction (see below). While the IR spectrum shows only absorptions in the area of terminal carbonyls, the $^{31}P\{^1H\}$-NMR spectrum shows three singlets for the three non equivalent phosphorus ligands. In the ^1H-NMR spectrum, apart from the cyclohexyl multiplet, **8** gives rise to two hydride resonances which show only hetero-spin coupling: The pseudo triplet at δ −8.64 ppm is attributed to H(2) which is coupled (5.5 Hz) with P(2) and P(3), the angles H(2)–Os(2)–P(2) [94(2)°] and H(2)–Os(3)–P(3) [97(2)°] being very similar and small. The doublet of doublets at δ −12.87 ppm assigned to H(1), is also coupled to P(2) (8 Hz) and to P(3) (38 Hz), the angles H(1)–Os(2)–P(2) and H(1)–Os(3)–P(3) being different (83.9(2) and 169.7(2)°, respectively) (Fig. 5).

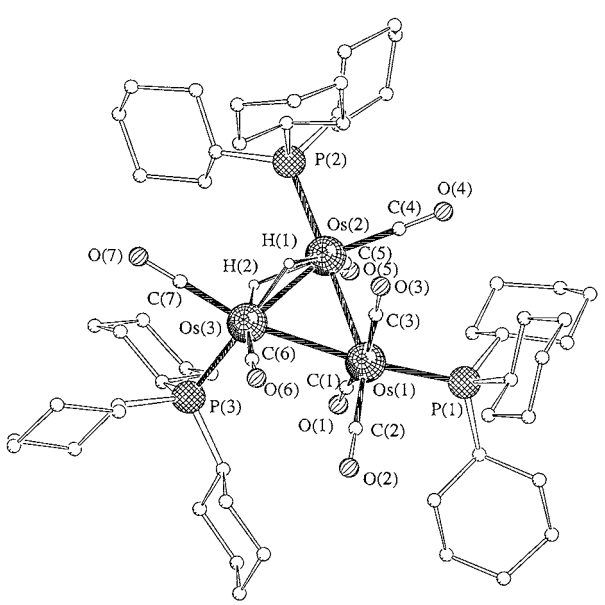

Fig. 5. Molecular structure of $H_2Os_3((CO)_7(PCy_3)_3$ (**8**). The hydrogen atoms of the cyclohexyl groups have been omitted for clarity.

Table 3
Selected bond lengths (Å) and angles (°) for $H_2Os_3(CO)_7(PCy_3)_3$ (**8**)

Bong lengths[a]		Angles[a]	
Os(1)–Os(2)	2.8881(2)	Os(2)–Os(1)–Os(3)	56.00(3)
Os(1)–Os(3)	2.8920(2)	Os(3)–Os(2)–Os(1)	62.07(3)
Os(2)–Os(3)	2.7135(2)	Os(2)–Os(3)–Os(1)	61.93(3)
Os(1)–P(1)	2.395(2)	H(1)–Os(2)–P(2)	83.9(2)
Os(2)–P(2)	2.371(2)	H(2)–Os(2)–P(2)	94(2)
Os(3)–P(3)	2.364(2)	H(1)–Os(3)–P(3)	169.7(2)
Os(2)–H(1)	1.72(7)	H(2)–Os(3)–P(3)	97(2)
Os(3)–H(1)	1.77(7)	C(1)–Os(1)–P(1)	89.2(2)
Os(2)–H(2)	1.88(6)	C(2)–Os(1)–P(1)	93.0(2)
Os(3)–H(2)	1.92(6)	C(3)–Os(1)–P(1)	98.3(3)
Os(1)–C(1)	1.924(8)	C(4)–Os(2)–P(2)	90.9(2)
Os(1)–C(2)	1.873(8)	C(5)–Os(2)–P(2)	96.3(2)
Os(1)–C(3)	1.933(9)	C(6)–Os(3)–P(3)	92.5(3)
Os(2)–C(4)	1.87(1)	C(7)–Os(3)–P(3)	87.7(3)
Os(2)–C(5)	1.878(9)		
Os(3)–C(6)	1.89(1)		
Os(3)–C(7)	1.863(8)		

[a] Estimated standard deviations in parantheses.

The single-crystal X-ray structure analysis of **8** reveals a tri-osmium framework with three phosphine ligands. All carbonyl ligands are terminal, and two μ_2-hydride ligands are positioned on the same Ru–Ru edge. The three osmium atoms define an isosceles triangle in which the non-bridged osmium–osmium distances are 2.881(2) Å (Os(1)–Os(2)) and 2.8920 Å (Os(1)-Os(3)), they are longer that in the parent complex $H_2Os_3(CO)_{10}$ (average 2.815 Å) [40]. The short dihydrido-bridged osmium-osmium bond is 2.7135(2) Å, slightly longer than the corresponding distance in the parent compound $H_2Os_3(CO)_{10}$ (2.681 Å) [40] and in the mono-substituted derivatives $H_2Os_3(CO)_9(PPh_3)$ (2.683(2) Å) [41], $H_2Os_3(CO)_9(PPr^i_3)$ (2.689(1) Å) [42] and $H_2Os_3(CO)_9(PMe_2Ph)$ (2.703(1) Å) [43]. Two phosphine ligands are equatorial, and one is axial. The osmium–phosphine distances (average 2.377 Å) are similar to that observed in $H_2Os_3(CO)_9(PPh_3)$ (2.361(2) Å) [41], $H_2Os_3(CO)_9(PPr^i_3)$ (2.384(5) Å) [42] and $H_2Os_3(CO)_9(PMe_2Ph)$ (2.347 Å) [43] (Table 3).

3. Theoretical analysis of the 44 e$^-$ Ru_3 species

In order to shed some light on the electronic structure and the bonding of the 44 e$^-$ cluster **3**, we have performed extended Hückel theory (EHT) and density functional theory (DFT) molecular orbital (MO) calculations on the isoelectronic models $H_2Ru_3(CO)_9$ and $H_2Ru_3(CO)_6(PH_3)_3$. The choice of the former hypothetical cluster comes from its hight ideal D_{3h} symmetry which allows an easier MO analysis (see below). Details of the calculations are given in Section 4.

3.1. Stereochemical considerations

Before entering into a detailed analysis of the MO calculations, we would like to point out some important structural similarities and differences existing between the electron deficient cluster $H_2Ru_3(CO)_6(PCy_3)_3$ and classical triangular 48 e^- compounds such as $Ru_3(CO)_{12}$ [17] or **5**. Discarding for the moment the hydrogen atoms in **3**, one can say that in both types of clusters the Ru atoms are in a similar tetracoodinated ligand environment. This ML_4-type local environment of approximate C_{2v} symmetry is often described as derived ideally from an octahedral ML_6 system from which two *cis* ligands have been removed [44,45]. In such a fragment, one of the LML angles is large, approaching the ideal value of 180°. In a 48 e^- species such as $Ru_3(CO)_{12}$, the almost linear LML arrangements are perpendicular to the Ru_3 plane, while in **3** they lie in the Ru_3 plane, the corresponding ligands being the bridging carbonyls. This different orientation of the same ligand environment in both types of complexes is sketched in the bottom of Fig. 6.

3.2. Comparison of the bonding in the 44 e^- model $[Ru_3(CO)_9]^{2-}$ and the 48 e^- cluster $Ru_3(CO)_{12}$

The frontier orbitals of a C_{2v} octahedron-derived ML_4 unit are well known [44,45]. They are shown in the middle of Fig. 6 for the two considered orientations of the fragments. They consist in a set of five orbitals: The highest is a σ-type hybrid, lying above a π-type hybrid, situated above a group of three closely spaced d-type levels, derived from the t_{2g} orbitals of the ML_6 parent, which are of σ-, δ- and π-type, respectively. Note that this latter π orbital is perpendicular to the π-type hybrid. The more diffuse and better oriented hybrids generally provide stronger interactions than the three d-type levels.

In a 48 e^- cluster of D_{3h} symmetry, the way the frontier orbitals of the three metal centers interact is qualitatively schematized on the left side of Fig. 6, as obtained from EHT calculations on $Ru_3(CO)_{12}$. The three metallic σ-type hybrids mix to give an in-phase $2a'_1$ and two out-of-phase 3e′* combinations. Lying in the Ru_3 plane, the other hybrid is also of σ-type with respect to Ru–Ru bonding. It is labelled π_s in Fig. 6. The d-type π orbital, which is perpendicular to the Ru_3 plane is labelled $\pi_\perp$. The π_σ frontier orbitals mix to give two bonding 2e′ and one antibonding $1a_2''$* MO's. Similarly, the d-block leads to combinations of σ-type ($1a'_1$ and 1e′*), of δ-type (1e″ and $1a_1''$*) and of $\pi_\perp$ ($1a_2''$ and $2e_2''$*). At the Ru–Ru separation of ca. 2.9 Å, the nine d-type combinations are only weakly bonding or antibonding and therefore remain at the rather low energy of a non-bonding d-type level. This is not the case for the hybrid combinations 3e′* and $1a_2''$* which are high-lying antibonding levels. In a 48 e^- cluster, there are 8 electrons per metal center available for filling the metal combinations. Twelve metallic orbitals of $Ru_3(CO)_{12}$ will be filled, leaving a large HOMO/LUMO gap separating the three bonding and nine more-or-less non-bonding orbitals from the three antibonding ones (2.04

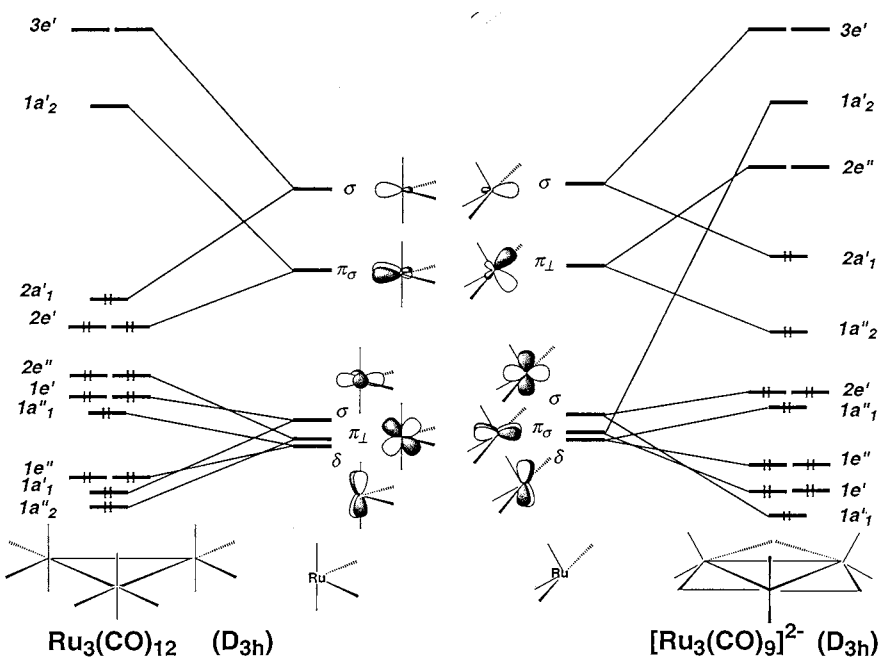

Fig. 6. Simplified MO diagrams of $Ru_3(CO)_{12}$ (left) and $[Ru_3(CO)_9]^{2-}$ (right) based on the interaction of the frontier orbitals of the three metal centres considered as octahedrally-derived ML_4 'monomers'. The second-order mixing between combinations of the same symmetry is not considered.

eV from EHT calculations). Considering all the other occupied levels as nonbonding, the three occupied bonding combinations of the hybrid orbitals, namely 2e′ and $2a_1'$ in Fig. 6, can be associated with the three 2-electron 2-center Ru–Ru bonds. The computed EHT Ru–Ru overlap population is 0.216, a value in agreement with a bond order of 1.

We now apply the same symmetry considerations to the 44 e^- deprotonated model of $H_2Ru_3(CO)_9$, namely the D_{3h} fragment $[Ru_3(CO)_9]^{2-}$. As compared to $Ru_3(CO)_{12}$, the different orientation of the local ligand environment around the metal atoms exchanges the roles of the two π-type frontier orbitals (see Fig. 6). The hybrid is now $\pi_\perp$, leading to the 2e″* and $1a_2''$ combinations, while the now in-plane π_σ d-level gives rise to the 1e′ and $1a_2''$* combinations. Due to the good overlap ability of the involved hybrid and to the shorter Ru–Ru bonds, the $\pi_\perp$ interaction is much stronger than in $Ru_3(CO)_{12}$. EHT calculations indicate that the π_σ interaction is also significant. The other metallic frontier orbitals, of σ and δ local symmetries, barely unchanged upon the rotation of the local metallic framework, interact more or less similarly (i.e. weakly) as in $Ru_3(CO)_{12}$. The resulting level ordering of the $[Ru_3(CO)_9]^{2-}$ fragment is schematized on the right side of Fig. 6, as obtained from EHT calculations. In $[Ru_3(CO)_9]^{2-}$, there are 20 electrons left available for filling the metal combinations. For this electron count, the two highest occupied MO's are the $2a_1'$ and $1a_2''$ bonding combinations of the two high-lying hybrids. Comparing the metallic configurations of the 48 e^- $Ru_3(CO)_{12}$ and 44 e^- $[Ru_3(CO)_9]^{2-}$ systems (Fig. 6), it appears that the main difference is that the 2e″* out-of-phase $\pi_\perp$ combination is almost nonbonding and populated in the former but significantly antibonding and unoccupied in the latter. As a result, $[Ru_3(CO)_9]^{2-}$ contains three σ-type bonding electron pairs (located in the $2a_1'$ HOMO and in the 1e′ π_σ combination) and one π-type significantly bonding pair in the $1a_2''$ level. This situation corresponds to a Ru–Ru bond order of 4/3. The corresponding EHT overlap population is 0.279, a value in agreement with a bond order larger than 1. $[Ru_3(CO)_9]^{2-}$ could be described simply with three equivalent canonical formulae exhibiting two R–Ru single bonds and one Ru=Ru double bond, with one electron-pair vacancy on the singly bonded Ru atom. The computed EHT HOMO/LUMO gap of $[Ru_3(CO)_9]^{2-}$ (0.71 eV) is not very large suggesting some instability. As shown below, the presence of two capping hydrogen atoms brings significant additional stability to the cluster.

3.3. The 44 e^- model $H_2Ru_3(CO)_9$

The EHT MO diagram of $H_2Ru_3(CO)_9$ is shown in Fig. 7, based on the interaction of $[Ru_3(CO)_9]^{2-}$ (left side) with the $(H\cdots H)^{2+}$ bicapping fragment (right side) and assuming D_{3h} symmetry. The skeletal orbitals of the $[Ru_3(CO)_9]^{2-}$ unit have been described above. The frontier orbitals of the $(H\cdots H)^{2+}$ fragment are very simple. They are the in-phase (a_1') and out-of-phase (a_2') combinations of the 1s hydrogen orbitals, which are somewhat split due to the weak H···H overlap (H···H distance = 2.1 Å). They are vacant in the considered charge partitioning. Calculations indicate that they interact with the two highest occupied orbitals of $[Ru_3(CO)_9]^{2-}$, $2a_1'$ and $1a_2''$, which have the proper symmetry and a localization to favor strong overlap. The occupation after interaction of the a_1' and a_2'' orbitals of the $[Ru_3(CO)_9]^{2-}$ fragment is 0.74 and 0.85, respectively. Being strongly Ru–Ru bonding, their depopulation upon interaction reduces the Ru–Ru overlap population to 0.096. This value is probably largely underestimated at the EHT level. Nevertheless, it is indicative of a significant electron transfer from the Ru–Ru bonds to the hydrogen atoms. The resulting net charge on the hydrogen atoms is −0.24 conferring to these atoms some hydrido character. The Ru–H overlap population is rather large (0.202). Interestingly, the H···H overlap population is very small, but positive (+0.002). Because of their strong interactions with their hydrogen counterparts, the $2a_1'$ and $1a_2''$ orbitals of $[Ru_3(CO)_9]^{2-}$ are destabilized strongly, leaving a large HOMO/LUMO gap (1.81 eV) for the $H_2Ru_3(CO)_9$ cluster, in full agreement with the stability of the isoelectronic cluster **3**.

DFT calculations performed on $H_2Ru_3(CO)_9$ at the LDA level (see computational details) fully confirm the EHT MO qualitative analysis. Full geometry optimization without any symmetry constraint indicates no significant departure from the D_{3h} symmetry. One can see on the left side of Fig. 8 that the EHT and DFT one-electron level orderings are in a very good agreement, with similar HOMO–LUMO gaps. The major optimized bond distances are reported in Table 4. They are in satisfying agreement with the X-ray data of **3**, except for the Ru–Ru distances which are computed to be somewhat longer than the experimental ones (by ≈ 0.08 Å). The introduction of gradient corrections in the calculations (see computational details) does not change significantly these results.

3.4. The $H_2Ru_3(CO)_6(PH_3)_3$ model

Going from $H_2Ru_3(CO)_9$ to the less symmetrical cluster $H_2Ru_3(CO)_6(PH_3)_3$ does not change the major features of the bonding and electronic structure. EHT calculations were performed of the latter model assuming both the experimental structure of **3** and an averaged idealized geometry of C_s symmetry. Since only small insignificant differences were found between both calculations, we discuss below the results corresponding

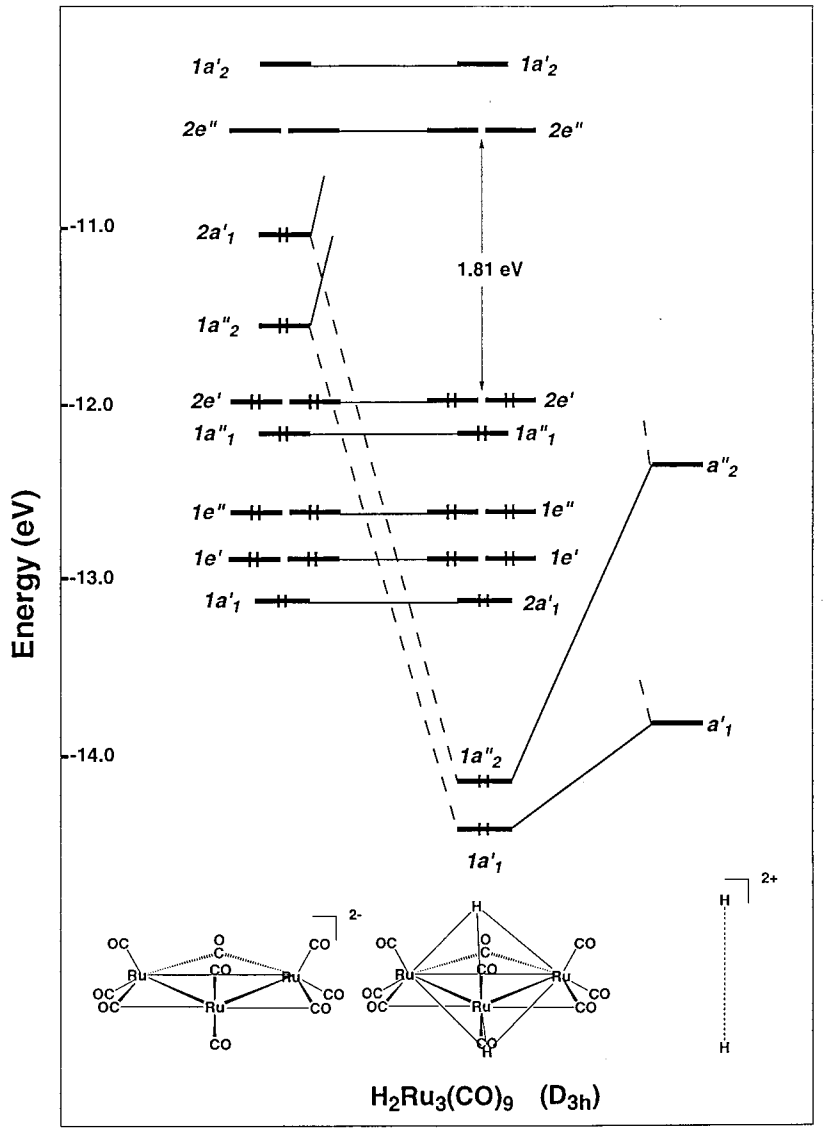

Fig. 7. Molecular orbital interaction diagram of $H_2Ru_3(CO)_9$ from EHT calculations.

to the C_s geometry. The HOMO–LUMO gap (1.60 eV) is of the same order of magnitude as the one computed for $H_2Ru_3(CO)_9$. The averaged Ru–Ru and Ru–H overlap populations, respectively 0.094 and 0.202 are also quite similar. DFT geometry optimization of $H_2Ru_3(CO)_6(PH_3)_3$ under the constraint of C_s symmetry lead to a similar level ordering (see Fig. 8) and HOMO–LUMO gap. The corresponding bond distances are listed in Table 4 in which the atoms are labelled as in the X-ray structure of **3** (see Fig. 2). The agreement with the X-ray data of **3** is good, with the Ru–Ru distances closer to the experimental values than to that computed for $H_2Ru_3(CO)_9$. The range of the Ru–H optimized distances (1.92–1.98 Å) is smaller than the corresponding experimental one found for **3** (1.61–2.04 Å). It is likely that the X-ray values are less accurate than the theoretical ones. H(1), which is close to two phosphine ligands is less tightly bonded than H(2) which is close to only one phosphine. Although the DFT calculations do not modelize the steric hindrance of the bulky PCy_3 phosphines, these results suggests a rather symmetrical μ_3-bonding of both hydrogen atoms in **3**.

3.5. Comparison with other electron deficient triangular clusters

From the above analysis one can describe the 44 e^- cluster **3** or its hypothetical relative $H_2Ru_3(CO)_9$ as a symmetrically protonated trinuclear system having three σ-bonds, one delocalized π-bond and one delocalized electron-pair vacancy. The difference with the 46 e^- clusters **8** and $H_2Os_3(CO)_{10}$ is that the latter have no electron vacancy and present a localized double bond

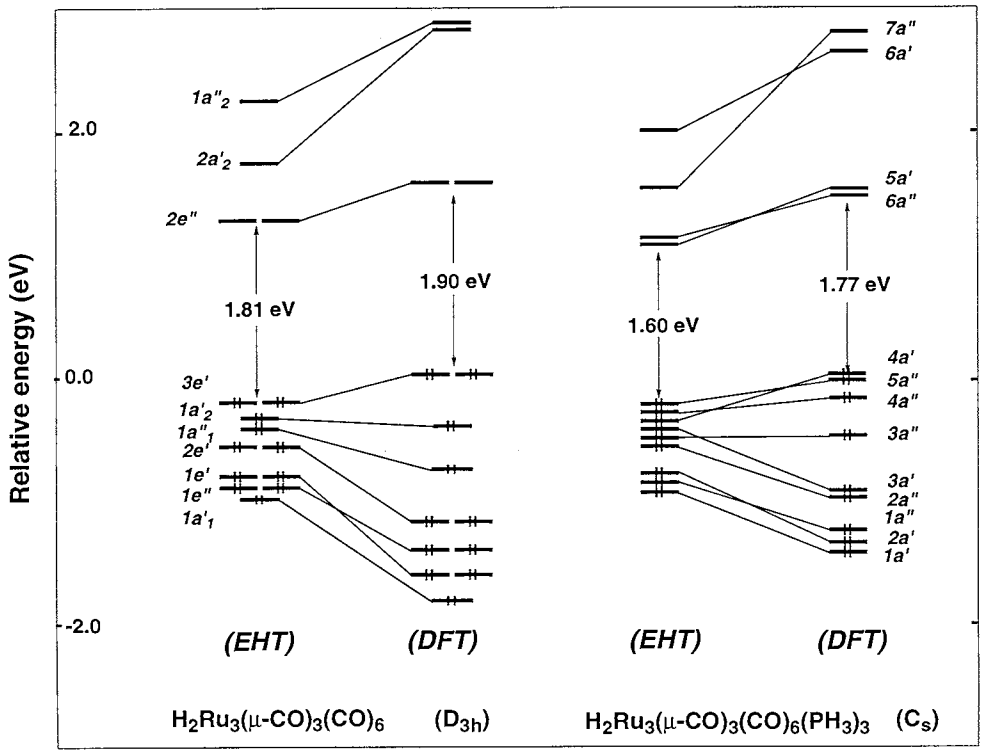

Fig. 8. EHT and DFT one-electron level ordering of $H_2Ru_3(CO)_9$ (left) and $H_2Ru_3(CO)_6(PH)_3$ (right).

which is bridged by the protons. One may wonder why the double bond is not localized in the 44 e^- systems. Although the potential energy surfaces of the $H_2Ru_3(CO)_6L_3$ (L=CO, PH_3) models were not explored fully, our calculations suggest that stability is favored by the presence of three bridging carbonyls which in turns favour π-delocalization.

As stated above, **3** is not the only 44 e^- triangular cluster characterized so far. Several 44 e^- Pd and Pt compounds are known [19–28]. Although they possess the same number of electrons, their electronic structure is different. In most of these compounds the local ligand environment is planar. Assuming a 16 e^- count per metal center, the existence of three M–M single bonds would correspond to 42 e^- for the whole cluster. Thus, the 44 e^- Pd_3 and Pt_3 planar or near-planar systems [19–27] are electron rich with respect to this count. Previous calculations [46,47] have shown that they bear three σ-bonding pairs (in MOs of e′ and a_1' symmetry) and one σ-antibonding pair (in a MO of a_2' symmetry). This latter orbital is high-lying and vacant in the Ru_3 systems (see Figs. 6 and 7). Some of the above-mentioned clusters have only two metal centers lying in a planar environment [20,23,27,28]. They are better described as resulting from the assembly of two 16 e^- Pt centers and one 18 e^- Fe center, which corresponds to a localized M–M bonding with three σ-bonding pairs. Nevertheless, without any significant M–M π-bonding, none of these 44 e^- clusters is electronically similar to **3**.

The group VIb 44 e^- bicapped triangular clusters $Cr_3(\mu_3\text{-}S)_2(\mu\text{-}S)_3(dppe)_3$, $[Mo_3(\mu_3\text{-}S)_2(\mu\text{-}S)_3(\mu\text{-}Cl)_3Cl_6]^{3-}$ and $Mo_3(\mu_3\text{-}S)_2(\mu\text{-}S)_3(PMe_3)_6$ have also an electronic configuration different from that of **3** [29–32]. They have been shown to bear three σ-bonding pairs and one non-bonding δ-type combination of a_1'' or e″ symmetry

Table 4
Major DFT-optimized bond distances of $H_2Ru_3(\mu\text{-}CO)_3(CO)_6$ and $H_2Ru_3(\mu\text{-}CO)_3(CO)_3(PH_3)_3$]

	$H_2Ru_3(\mu\text{-}CO)_3(CO)_6$ (D_{3h})	$H_2Ru_3(\mu\text{-}CO)_3(CO)_3(PH_3)_3$ (C_s)
Ru(1)–Ru(3)	2.760	2.736
Ru(2)–Ru(1,3)		2.733
Ru(2)–H(1)	1.960	1.917
Ru(1,3)–H(1)		1.984
Ru(2)–H(2)		1.985
Ru(1,3)–H(2)		1.931
Ru(2)–C(2,3)	2.147 (bridg.)	2.133
Ru(1,3)–C(3,2)		2.145
Ru(1,3)–C(1)		2.132
Ru(2)–C(6)	1.884 (term.)	1.856
Ru(1,3)–C(4,5)		1.862
Ru(2)–P(3)		2.269
Ru(1,3)–P(1,2)		2.278
C(1)–O(1)	1.160 (bridg.)	1.156
C(2,3)–O(2,3)		1.170
C(4,5)–O(4,5)	1.146 (term.)	1.156
C(6)–O(6)		1.157
H···H	2.281	2.281

[29,30,48]. On the other hand, the monocapped species $[W_3(\mu_3\text{-}O)(Oac)_6(H_2O)_3]^{2+}$ has been shown to possess three σ-type W–W bonding pairs and an additional weakly bonding σ-type pair [32]. Clearly, among all the 44 e^- trinuclear systems, cluster **3** is so far unique with respect to bonding and electronic configuration.

4. Experimental

4.1. General methods

The reactions were performed under nitrogen using standard Schlenk or vacuum-line techniques. The organic solvents were refluxed over appropriate desiccants [49], distilled and saturated with nitrogen prior to use. The NMR spectra were recorded on a Varian Gemini 200 BB instrument or on a Brucker AMX 400, chemical shifts were measured relative to $SiMe_4$ (^1H, ^{13}C) and to 85% H_3PO_4 (^{31}P). The IR spectra were recorded with a Perkin–Elmer FT IR 1720X spectrometer (4000–400 cm^{-1}). Micro-analytical data were obtained from the Mikroelementaranalytisches Laboratorium der ETH Zürich. Mass spectra were obtained with a LCQ Finnigan instrument using the ESI method. The starting compounds $[Na][HRu_3(CO)_{11}]$ [50,51] and $[PPN][HOs_3(CO)_{11}]$ [52] were synthesised according to the published methods. Tricyclohexylphosphine was purchased from Aldrich and used without further purification.

4.2. Synthesis of $H_2Ru_3(CO)_6(PCy_3)_3$ (3)

$Ru_3(CO)_{12}$ (0.200 g, 0.31 mmol) was dissolved in 20 ml of dry THF, an excess of $NaBH_4$ was added. The solution was stirred at room temperature for 30 min and then filtered. The THF was evaporated and the remaining $[Na][HRu_3(CO)_{11}]$ was dissolved in 30 ml of MeOH. After addition of tricyclohexylphosphine (0.33 g, 1.2 mmol), the solution was heated to reflux (110°C bath temperature) in a Schlenk tube connected to a reflux condenser for 1 h. The product **3** precipitated directly from the reaction solution during the reaction as a purple powder. The solution was filtered hot, and the solid product was recrystallised from dichloromethane–methanol to give dark red, block-shaped crystals which are slightly air-sensitive (0.30 g, 73%).

IR(CH_2Cl_2): ν(CO) 2027vw, 1949m, 1917vs, 1871w, 1855w, 1819vs, 1757w cm^{-1}; ^{1}H-NMR ($CDCl_3$): δ 1.27–2.30 (99H, m, C_6H_{11}), −19.46 [1H, dtd, J(H1–P3) = 28.3 Hz, J(H1–P1,P2) = 5.3 Hz, J(H1–H2) = 2.2 Hz, μ^3-H1], −21.02 [1H, tdd, J(H2–P1,P2) = 26.4 Hz, J(H2–P3) = 5.4 Hz, J(H1–H2) = 2.1 Hz, μ^3-H2], $^{31}P\{^1H\}$-NMR ($CDCl_3$): δ 74.8 (s, 1P), 71.3 (s, 2P) no coupling observed; FAB-MS: m/z 1316 (based on ^{102}Ru); Found: C 53.63, H 7.45; Calc. for $C_{60}H_{101}O_6P_3Ru_3$ 2 H_2O: C 53.36, H 7.84.

4.3. Synthesis of $Ru_3(CO)_9(PCy_3)_3$ (5)

$Ru_3(CO)_{12}$ (0.150 g, 0.23 mmol) was dissolved in 20 ml of dry THF, an excess of $NaBH_4$ was added. The solution was stirred at room temperature for 30 min, then filtered and transferred into a pressure Schlenk tube. The THF was evaporated, the remaining $[Na][HRu_3(CO)_{11}]$ was dissolved in 30 ml of MeOH. After addition of tricyclohexylphosphine (0.33 g, 1.2 mmol), the solution was heated for 1 h in the closed vessel (80°C bath temperature). The product **5** precipitated directly from the reaction solution during the reaction as a purple powder which was filtered off hot and recrystallised from dichloromethane–methanol to give dark red, air-stable, cube-like crystals which contain two water molecules (from methanol) (0.18 g, 55%).

IR(CH_2Cl_2): ν(CO) 1959vs, 1949vs cm^{-1}; ^{1}H-NMR ($CDCl_3$): δ 1.29–2.04 (m, C_6H_{11}); ^{31}P-NMR ($CDCl_3$): δ 47.3 (s, PCy_3); FAB-MS: m/z 1398 (related to ^{102}Ru); Found: C 52.64, H 7.00; Calc. for $C_{63}H_{99}O_9P_3Ru_3$ 2 H_2O: C 52.82, H 7.25.

4.4. Synthesis of $H_2Os_3(CO)_7(PCy_3)_3$ (8)

$[PPN][HOs_3(CO)_{11}]$ (0.20 g, 0.14 mmol) was dissolved in 50 ml of MeOH. After addition of tricyclohexylphosphine (0.19 g, 0.7 mmol) the solution was heated for 3 h to reflux in a Schlenk tube equipped with a reflux condenser (110°C bath temperature). The product **8** precipitated directly from the reaction solution during the reaction as a green–yellow powder which was filtered off and recrystallised from dichloromethane–methanol to give green, air-stable crystals (0.17 g, 75%).

IR(CH_2Cl_2): ν(CO) 2001w, 1969vs, 1942w, 1923s, 1907m cm^{-1}; ^{1}H-NMR ($CDCl_3$): δ 1.27–2.09 (99H, m, C_6H_{11}), −8.64 [1H, t, J(H–P) = 5.5 Hz, μ^2-H2); −12.87 [1H, dd, J(H–P) = 38 Hz, J(H–P) = 8 Hz, μ^2-H1], $^{31}P\{^1H\}$-NMR ($CDCl_3$): δ 37.5 (s, 1P), 21.8 (s, 1P), 14.2 (s, 1P), no coupling observed; FAB-MS: m/z 1610 (based on ^{190}Os); Found: C 43.79, H 5.98; Calc. for $C_{61}H_{101}O_7Os_3P_3CH_2Cl_2$: C 43.93, H 6.12.

4.5. Reaction of $H_2Ru_3(CO)_6(PCy_3)_3$ (3) with CO

The complex $H_2Ru_3(CO)_6(PCy_3)_3$ (0.100 g, 76.2 μmol) was dissolved in 20 ml of CH_2Cl_2 in a pressure Schlenk tube, which was pressurised with 1.5 bar of carbon monoxide. The solution was stirred at room temperature until the colour of the solution became red. Then the solution was evaporated to dryness. The residue contained **4**.

IR(CH_2Cl_2): 2071w, 2026w, 1997s cm^{-1}; ^{1}H-NMR (C_6D_6): δ 1.27–2.22 (99H, m, C_6H_{11}), −10.89 [1H, d, J(H–P) = 10 Hz], −17.94 [1H, dd, J(H–P) = 20.2 Hz, J(H–P) = 7.6 Hz]; ^{31}P-NMR (C_6D_6): δ 64.7 (m, 1P), 32.9 (m, 1P), 11.4 (m, 1P), no coupling observed; FAB-MS: m/z 1372 (based on ^{102}Ru).

4.6. Reaction of $Ru_3(CO)_9(PCy_3)_3$ (5) with H_2

The complex $Ru_3(CO)_9(PCy_3)_3$ (0.100 g, 71.7 μmol) was dissolved in 20 ml of CH_2Cl_2 in a closed pressure Schlenk tube, which was pressurised with 1.5 bar of hydrogen. The solution was stirred at room temperature until the colour of the solution became red. Then the solution was evaporated to dryness. The residue contained **4**.

IR(CH_2Cl_2): 2071w, 2026w, 1997s cm^{-1}; ^{1}H-NMR (C_6D_6): δ 1.27–2.22 (99H, m, C_6H_{11}), −10.89 [1H, d, J(H–P) = 10 Hz], −17.94 [1H, dd, J(H–P) = 20.2 Hz, J(H–P) = 7.6 Hz]; ^{31}P-NMR (C_6D_6): δ 64.7 (m, 1P), 32.9 (m, 1P), 11.4 (m, 1P), no coupling observed; FAB-MS: m/z 1372 (based on ^{102}Ru).

4.7. Crystal structure of $H_2Ru_3(CO)_6(PCy_3)_3$ (3)

Intensity data for an orange crystal of **3** were collected using a Stoe imaging plate diffractometer system (Stoe and Cie, 1995) equipped with a one-circle goniometer and a graphite-monochromator. Data collection was performed using Mo–K_α radiation ($\lambda = 0.71073$ Å). 200 exposures (3 min per exposure) were obtained at 70 mm with $0 < \varphi < 200°$ and with the crystal oscillated through 1° in φ. The structure was solved by direct methods using the program SHELXS-97 [53] and refined by full matrix least squares on F^2 with SHELXL-97 [54]. The positions of the two hydrides were derived from Fourier difference maps and refined while the remaining hydrogen atoms were included in calculated positions and treated as riding atoms using SHELXL-97 default parameters. Crystallographic details are given in Table 4 and significant bond lengths and bond angles are listed in Table 1. The figure was drawn with SCHAKAL [55].

4.8. Crystal structure of $Ru_3(CO)_9(PCy_3)_3$ (5)

Suitable crystals of **5** were obtained as indicated in the synthetic section. Intensity data were collected on a Stoe–Siemens AED2 4-circle diffractometer at −50°C (Mo–K_α, graphite monochromated radiation, λ = 0.71073 Å; $\omega/2\theta$ scans). Table 1 summarises the crystallographic and selected experimental data for **5**. The structure was solved by direct methods using the program SHELXS-86 [56]. The refinement, using weighted full-matrix least-square on F^2, was carried out using the program SHELXL-93 [57]. No absorption correction was applied. The hydrogen atoms of the cyclohexylphosphine ligands were included in calculated positions and treated as riding atoms using the SHELXL 93 default parameters. One disordered molecule of methanol and five molecules of water were found per asymmetric unit. Crystallographic details are given in Table 4 and significant bond lengths and bond angles are listed in Table 2. The figure was drawn with SCHAKAL 92 [55]. Full tables of atomic parameters and bond lengths and angles may be obtained from the Cambridge Crystallographic Data Centre, 12 Union Road, Cambridge CB2 1EZ (UK) on quoting the full journal citation.

4.9. Crystal structure of $H_2Os_3(CO)_7(PCy_3)_3$ (8)

A green crystal of compound **8** was mounted on a Stoe–Siemens AED2 four-circle diffractometer. Intensity data were measured using graphite-monochromator Mo–K_α radiation ($\lambda = 0.71073$ Å). The $\omega/2\theta$ scan technique was used to a maximum 2θ value of 50.0°. The cell parameters were determined from a least square treatment of the setting angles of 24 reflections with $12.2° < \theta < 17.2°$. The intensities of two representative reflections were measured every 60 min. During data collection the intensity of the standards decreased by less than 2%. A semi-empirical absorption correction was applied using psi-scans ($T_{min} = 0.22$, $T_{max} = 0.35$). The structure was solved by direct methods using the program SHELXS-97 [53] and refined by full matrix least squares on F^2 with SHELXL-97 [54]. The positions of the two hydrides both bridging Os2 and Os3 were derived from the Fourier difference maps and refined freely while the remaining hydrogen atoms were included in calculated positions and treated as riding atoms using SHELXL-97 default parameters. One disordered molecule of methanol was found per asymmetric unit and refined isotropically. Crystallographic details are given in Table 4 and significant bond lengths and bond angles are listed in Table 3. The figure was drawn with SCHAKAL [55] (Table 5).

4.10. Computational details

EHT calculations have been carried out within the extended Hückel formalism [58] assuming the weighted H_{ij} formula [59] with the CACAO package [60]. The exponents (ξ) and the valence shell ionization potentials (H_{ij} in eV) were (respectively): 1.3, −13.6 for H 1s; 1.625, −21.4 for C 2s; 1.625, −11.4 for C 2p; 2.275, −32.3 for O 2s; 2.275, −14.8 for O 2p; 1.6, −18.6 for P 3s; 1.6, −14.0 for P 3p; 2.078, −8.6 for Ru 5s, 2.043, −5.1 for Ru 5p. H_{ij} value for Ru 4d was set equal to −12.2. A linear combination of two Slater-type orbitals of exponents $\xi_1 = 5.378$ and $\xi_2 = 2.303$ with the weighting coefficients $C_1 = 0.5340$ and $C_2 = 0.6365$ was used to represent the Ru 4d atomic

Table 5
Crystal data and data collection parameters for **3**, **5** and **8**

Compound	**3**	**5**	**8**
Formula	$C_{60}H_{101}O_6P_3Ru_3 2H_2O$	$C_{63}H_{99}O_9P_3Ru_3 2H_2O$	$C_{61}H_{101}O_7Os_3P_3CH_3OH$
M	1314.53	1474.52	1641.97
Crystal size (mm)	$0.50 \times 0.25 \times 0.10$	$0.61 \times 0.46 \times 0.34$	$0.30 \times 0.30 \times 0.19$
Temperature (K)	223(2)	223(2)	293(2)
Crystal system	Monoclinic	Cubic	Triclinic
Space group	$P2_1/n$	$Pa\bar{3}$	$P\bar{1}$
Colour	Orange	Red	Green
a (Å)	10.561(1)	24.1347(12)	11.227(4)
b (Å)	36.649(2)	24.1347(12)	14.646(6)
c (Å)	15.957(1)	24.1347(12)	20.496(9)
α (°)	90	90	95.81(4)
β (°)	96.32(1)	90	93.26(3)
γ (°)	90	90	101.84(3)
Volume (Å^3)	6138.4(8)	14 058(12)	3 271(2)
Z	4	8	2
D_c (g/cm^3)	1.422	1.435	1.667
μ (mm^{-1})	0.854	0.765	5.935
$F(000)$	2 744	6 352	1 628
θ limits (°)	2.0.2 to 25.97	2.07 to 25.02	2.00 to 25.50
Reflections measured	38 984	4 157	12 165
Independent reflections	11 651	4 157	12 165
Observed reflections	6 231	3 224	9 953
Goodness-on-fit on F^2	0.801	1.186	1.135
R_1 [$I = 2\ \sigma(I)$]/R_1 (all data)	0.0487/0.1038	0.0579/0.0862	0.0434/0.0620
wR_2 [$I = 2\ \sigma(I)$]/wR_2 (all data)	0.0901/0.1028	0.1225/0.1727	0.0739/0.0825
residual e$^-$-density min/max (e/Å^3)	−0.781/1.276	−0.648/1.336	−0.885/1.065

orbitals. The following bond distances (Å) were used in the $H_2Ru_3(CO)_9$ (D_{3h}) and $H_2Ru_3(CO)_6(PH_3)_3$ (C_s) models: Ru–Ru = 2.694, Ru–μ-CO = 2.138, Ru–CO = 1.840, C–O = 1.150, Ru–P = 2.337, P–H = 1.420 Å and Ru–H = 1.876 Å.

DFT calculations [61–64] were carried out on the $H_2Ru_3(CO)_9$ and $H_2Ru_3(CO)_6(PH_3)_3$ models using the ADF program developed in the group of Baerends [65]. Electron correlation was treated within the local density approximation (LDA) [66]. Test calculations with non local density approximation (NLDA) [67,68] were carried out on $H_2Ru_3(CO)_9$ assuming D_{3h} symmetry. Since they led to very similar results, the LDA level was considered for all the calculated models. The numerical integration procedure applied for the calculations was developed by te Velde et al. [63]. The standard ADF STO basis set IV, of triple-ξ quality for the valence orbitals was used for all the atoms. The frozen-core approximation was considered [61].

5. Conclusions

It is interesting to note that the analogous cluster anions $[HRu_3(CO)_{11}]^-$ (**1**) and $[HOs_3(CO)_{11}]^-$ (**6**) react both with tricyclohexylphosphine in methanol solution to give the trisubstituted, electron-deficient, neutral clusters $H_2Ru_3(CO)_6(PCy_3)_3$ (**3**) and $H_2Os_3(CO)_7(PCy_3)_3$ (**8**), respectively. However, the ruthenium cluster **3** is a 44 e$^-$ system, while the osmium cluster **8** is a 46 e$^-$ system.

Acknowledgements

We thank the Fond National Suisse de la Recherche Scientifique for financial support of this work. Computing facilities were kindly provided by the IDRIS-CNRS computing center of Orsay (France). J.-Y.S. and M.T.G. are grateful to CNRS and to CONICYT for a cooperative French/Chilean travel grant. A generous loan of ruthenium trichloride hydrate by the Johnson Matthey Technology Centre (to G.S.-F.) is gratefully acknowledged.

References

[1] A.J. Deeming, in: E.W. Abel, F.G.A. Stone, G. Wilkinson (Eds.), Comprehensive Organometallic Chemistry II, Chapter 12, vol. 7, Pergamon, Oxford, 1995.
[2] M.I. Bruce, G. Shaw, F.G.A. Stone, J. Chem. Soc. Dalton Trans. (1972) 2094.
[3] M.I. Bruce, D.C. Kehoe, J.G. Matisons, B.K. Nicholson, P.H. Riegger, M.L. Williams, J. Chem. Soc. Chem. Commun. (1982) 442.

[4] M.I. Bruce, J.G. Matisons, B.K. Nicholson, J. Organomet. Chem. 247 (1983) 321.
[5] C.E. Kampe, N.M. Boag, C.B. Knobler, H.D. Kaesz, Inorg. Chem. 23 (1984) 1390.
[6] G. Lavigne, H.D. Kaesz, J. Am. Chem. Soc. 106 (1984) 4647.
[7] B.F.G. Johnson, J. Lewis, D. Pippard, J. Organomet. Chem. 160 (1978) 263.
[8] B.F.G. Johnson, J. Lewis, D. Pippard, J. Chem. Soc. Dalton. Trans. (1981) 407.
[9] H.C. Böttcher, G. Rheinwald, H. Stoeckli-Evans, G. Süss-Fink, J. Organomet. Chem. 469 (1994) 163.
[10] H.C. Böttcher, H. Thönnessen, P.G. Jones, R. Schmutzler, J. Organomet. Chem. 520 (1996) 15.
[11] S.A. Maclaughlin, A.J. Carty, N.J. Taylor, Can. J. Chem. 60 (1982) 87.
[12] S. Rivomanana, G. Lavigne, N. Lugan, J.-J. Bonnet, Inorg. Chem. 30 (1991) 4110.
[13] N. Nagashima, T. Fukahori, K. Aoki, K. Itoh, J. Am. Chem. Soc. 115 (1993) 10430.
[14] G. Süss-Fink, G. Rheinwald, H. Stoeckli-Evans, Inorg. Chem. 35 (1996) 3081.
[15] N.E. Leadbeater, J. Lewis, P.R. Raithby, J. Organomet. Chem. 543 (1997) 251.
[16] G. Süss-Fink, I. Godefroy, V. Ferrand, A. Neels, H. Stoeckli-Evans, J. Chem. Soc. Dalton Trans. (1998) 515.
[17] M.R. Churchill, F.J. Hollander, J.P. Hutchinson, Inorg. Chem. 16 (1977) 2655.
[18] F.A. Cotton, B.E. Hanson, J.D. Jamerson, J. Am. Chem. Soc. 99 (1977) 6588.
[19] S. Otsuka, Y. Tatsuno, M. Miki, T. Aoki, M. Matsumoto, H. Yoshioka, K. Nakatsu, J. Chem. Soc. Chem. Commun. (1973) 445.
[20] A. Albinati, G. Carturan, A. Musco, Inorg. Chim. Acta 16 (1976) L3.
[21] A.M. Arif, D.E. Heaton, R.A. Jones, C.M. Nunn, Inorg. Chem. 26 (1987) 4228.
[22] R. Bender, P. Braunstein, A. Dedieu, P. Ellis, B. Huggins, P.D. Harvey, E. Sappa, A. Tiripichio, Inorg. Chem. 35 (1996) 1223.
[23] M.F. Hallam, N.D. Howells, D.M.P. Mingos, R.W.M. Wardle, J. Chem. Soc. Dalton Trans. (1985) 845.
[24] S.G. Bott, M.F. Hallam, O.J. Ezomo, D.M.P. Mingos, I.D. Williams, J. Chem. Soc. Dalton Trans. (1988) 1461.
[25] G.W. Bushnell, K.R. Dixon, P.M. Moroney, A.D. Rattray, C. Wan, J. Chem. Soc. Chem. Commun. (1977) 709.
[26] D.E. Berry, G.W. Bushnell, K.R. Dixon, P.M. Moroney, C. Wan, Inorg. Chem. 24 (1985) 2625.
[27] R. Ramachandran, D.-S. Yang, N.C. Payne, R. Pudephatt, Inorg. Chem. 31 (1992) 4236.
[28] V.G. Albano, C. Ciani, J. Organomet. Chem. 66 (1974) 311.
[29] M.A. Arif, J.G. Hefner, R.A. Jones, T.A. Albright, S.-K. Kang, J. Am. Chem. Soc. 108 (1986) 1701.
[30] K. Tsuge, S. Yajima, H. Imoto, T. Saito, J. Am. Chem. Soc. 114 (1992) 7910.
[31] J. Huang, M. Shang, S. Lui, J. Lu, Sci. Sin. (Engl. Trans. 25 (1982) 1270.
[32] M. Ardon, F.A. Cotton, Z. Dori, A. Fang, M. Kapon, G.M. Reisner, M. Shaia, J. Am. Chem. Soc. 104 (1982) 5394.
[33] M.I. Bruce, M.J. Liddell, O. bin Shawkataly, C.A. Hughes, B.W. Skelton, A.H. White, J. Organomet. Chem. 347 (1988) 207.
[34] J.B. Keister, J. Organomet. Chem. 190 (1980) C 36.
[35] L.R. Nevinger, J.B. Keister, J. Maher, Organometallics 9 (1990) 1900.
[36] S. Aime, W. Dastrù, R. Gobetto, A. Viale, Organometallics 17 (1998) 3182.
[37] B.F.G. Johnson, J. Lewis, P.A. Kilty, J. Chem. Soc. A (1968) 2859.
[38] S.A.R. Knox, J.W. Koepke, M.A. Andrews, H.D. Kaesz, J. Am. Chem. Soc. 97 (1975) 3942.
[39] A.J. Deeming, Adv. Organomet. Chem. 26 (1986) 1.
[40] M.R. Churchill, F.J. Hollander, J.P. Hutchinson, Inorg. Chem. 16 (1977) 2697.
[41] R.E. Benfield, B.F.G. Johnson, J. Lewis, P.R. Raithby, C. Zuccaro, Acta. Cryst. B35 (1979) 2210.
[42] L.J. Farrugia, J. Organomet. Chem. 394 (1990) 515.
[43] R.D. Adams, B.E. Segmüller, Cryst. Struct. Comm. 11 (1982) 1971.
[44] R. Hoffmann, Angew. Chem. Int. Ed. Engl. 21 (1982) 711.
[45] T.A. Albright, J.K. Burdett, M.-H. Whangbo, Orbital interactions in chemistry, Wiley, NY, 1985.
[46] D.J. Underwood, R. Hoffmann, K. Tatsumi, A. Nakamura, Y. Yamamoto, J. Am. Chem. Soc. 107 (1985) 5968.
[47] D.I. Gilmour, D.M.P. Mingos, J. Organomet. Chem. 302 (1986) 127.
[48] Y. Jiang, A. Tang, R. Hoffmann, J. Huang, J. Lu, Organometallics 4 (1985) 27.
[49] D.D. Perrin, W.L.F. Armarego, Purification of Laboratory Chemicals, 3rd edition, Pergamon, Oxford, 1988.
[50] B.F.G. Johnson, J. Lewis, P.R. Raithby, G. Süss(-Fink), J. Chem. Soc. Dalton. Trans. (1979) 1356.
[51] G. Süss-Fink, Inorg. Synth. 24 (1986) 168.
[52] K. Brugess, R.P. White, Inorg. Synth. 28 (1990) 236.
[53] G.M. Sheldrick, SHELXS-97, Program for crystal structure solution, University of Göttingen, Germany, 1997.
[54] G.M. Sheldrick, SHELXL-97, Program for crystal structure refinement, University of Göttingen, Germany, 1997.
[55] E. Keller, SCHAKAL, Program for the graphic representation of molecular and crystallographic models, University of Freiburg, Germany, 1992.
[56] G.M. Sheldrick, Acta Cryst. Sect A 46 (1990) 467.
[57] G.M. Sheldrick, SHELXL-93, University of Göttingen, Germany (1993).
[58] R. Hoffmann, J. Chem. Phys. 39 (1963) 1397.
[59] J.H. Ammeter, H.-B. Bürgi, J.C. Thibeault, R. Hoffmann, J. Am. Chem. Soc. 100 (1978) 3686.
[60] C. Mealli, D. Proserpio, J. Chem. Ed. 67 (1990) 399.
[61] E.J. Baerends, D.E. Ellis, P. Ros, Chem. Phys. 8 (1975) 41.
[62] E.J. Baerends, P. Ros, Int. J. Quantum Chem. S12 (1978) 169.
[63] P.M. Boerrigter, G. te Velde, E.J. Baerends, Int. J. Quantum Chem. 33 (1988) 87.
[64] G. te Velde, E.J. Baerends, J. Comput. Phys. 99 (1992) 84.
[65] Amsterdam Density Functional (ADF) program, version 2.0.1, Vrije Universiteit Amsterdam, 1996.
[66] S.D. Vosko, L. Wilk, M. Nusair, Can. J. Chem. 58 (1990) 1200.
[67] A.D. Becke, Phys. Rev. A38 (1988) 3098.
[68] J.P. Perdew, Phys. Rev. B33 (1986) 8822.